ELSEVIER

Catalysis Today 59 (2000) 163–177

CATALYSIS TODAY

www.elsevier.com/locate/cattod

# Catalytic combustion of methane on substituted barium hexaaluminates

P. Artizzu-Duart[a,1], J.M. Millet[b], N. Guilhaume[a], E. Garbowski[a,*], M. Primet[a]

[a] *LACE, Université Claude Bernard Lyon 1, 43 Boulevard du Onze Novembre 1918, 69622 Villeurbanne Cedex, France*

[b] *Institut de Recherches sur la Catalyse, 2 Avenue A. Einstein, 69626 Villeurbanne Cedex, France*

**Abstract**

A sol–gel method using metallic barium, aluminum alkoxides and metal nitrates has been used to synthesize barium hexaaluminate partially substituted by either manganese, iron or both metal ions. The β-alumina structure was obtained by calcination under oxygen at 1200°C. X-ray analysis revealed that formation of a pure single phase $BaM_xAl_{12-x}O_{19}$ occurred up to $x$=4 for Fe, $x$=3 for Mn and for $Fe_1Mn_1$ in the case of mixed substituted hexaaluminates. Incorporation of Mn in excess leads to another phase formation (manganese oxide or spinel). As far as the valence state of transition metal ions is concerned, the introduced Fe ions were always trivalent, whereas the Mn ones were either divalent or trivalent. In the latter case, the first Mn ions were introduced in the matrix essentially as $Mn^{2+}$ and only for $BaMn_3Al_9O_{19}$ does manganese exist exclusively as $Mn^{3+}$, the higher the Mn concentration, the higher the proportion of $Mn^{3+}$. All solids were aged at 1200°C under water and oxygen and showed a good thermal resistance. Activity for methane combustion has been measured for fresh and aged solids, light-off temperatures were observed in the 560–640°C range. However, the highest activity was obtained for catalysts containing either 3 Mn, 2 Fe or 1 Fe+1 Mn ions per unit cell. Temperature programmed reduction (TPR) under hydrogen has been used to correlate the catalytic activity with the amount of easily reducible species. 

*Keywords:* Catalytic combustion; Barium hexaaluminates; Manganese; Iron; Temperature programmed reduction; Sol–gel synthesis; Thermal stability

## 1. Introduction

The new regulations concerning the emission of pollutants in gaseous emissions are becoming more and more stringent. The catalytic combustion of gaseous fuels appears to be a powerful process for environmental protection [1]. A lot of work has been performed on the catalytic combustion of methane which is one of the cleanest way to obtain thermal energy without any harmful CO, $NO_x$ or unburned hydrocarbon emissions [2]. For such a catalysis, special devices are required, and due to high temperature needed for very high efficiency output like for gas turbine [3], thermally stable catalysts are required [4]. Among various ceramics stable at high temperature in the presence of water, hexaaluminates, also named β-alumina for historical reason [5], have been selected.

The formula of all hexaaluminates is $M_2O(M'O)$-$6Al_2O_3$, where M or M′ stand for alkaline or alkaline-earth metal. The structure is lamellar and consists of layers of spinel blocks separated by a monolayer of oxides issued from either bulky alkaline cations, or bulkier alkaline-earth ones [6]. Such a lamellar structure prevents any contact between spinel

* Corresponding author. Tel. +33-4-72-44-83-33; fax: +33-4-72-44-81-14.

*E-mail address:* edouard.garbowski@univ-lyon1.fr (E. Garbowski)

[1] Present address: Battelle, Geneva Research Center, 7 route de Drize, CH 1227, Carouge Geneva, Switzerland.

0920-5861/00/$ – see front matter 
PII: S0920-5861(00)00281-9

blocks. Spinels are organized as an f.c.c. structure of oxygen anions, where both octahedral and tetrahedral sites are more or less filled [7]. On the other hand, α-alumina has an h.c.p. structure of oxygen anions with $\frac{2}{3}$ octahedral sites occupied by aluminum cations [7,8]. Formation of α-alumina at the expense of other forms (γ, δ, etc.) needs a restructuring of all the anion layers. This is not possible for β-alumina due to the blocking introduced by the alkaline(-earth) cation [9]. So, transformation of alumina is not possible and sintering is strongly hindered: these mixed oxides are exceptionally stable [10], but they are also almost inactive except at very high temperature. The introduction of active transition metal ions in the structure may be very worthwhile for activity [11]. But substitution is not easy because of charge and radius stress locally introduced. The aim of the present study is to investigate the catalytic activity as well as the thermal stability of barium hexaaluminate substituted at various levels by Mn and Fe ions.

## 2. Preparation

A sol–gel method, derived from that already published by Arai and co-workers [12] was used. Different solids have been synthesized: the parent barium hexaaluminate matrix and the solids resulting from the substitution of 1–4 $Al^{3+}$ ions per unit cell by $Fe^{3+}$, $Mn^{3+}$ or both ions.

The required amounts of metallic barium and aluminum isopropoxide (Aldrich) were suspended into 2-propanol leading to a mixture of the two alkoxides which are only partly soluble. The suspension was refluxed for 3 h at 80°C, then cooled at room temperature. Hydrolysis of the metal alkoxides was performed with an under-stoichiometric amount of water, i.e., the $xH_2O/M(OiPr)_x$ ratio is equal to 0.5 according to Arai and co-workers [12]. For the iron containing solids, the required amount of $Fe(NO_3)_3{\cdot}9H_2O$ was dissolved into a water/2-propanol mixture and added during the hydrolysis step. For manganese containing solid, $Mn(NO_3)_2{\cdot}4H_2O$ was used. A gel was rapidly formed; it was kept at room temperature for 15 h. Solvents were removed by evaporation under reduced pressure. The obtained powders were dried for a few hours at 120°C. They were finally calcined under flowing oxygen at 1200°C for 24 h. Such a treatment leads to "fresh catalysts".

## 3. Physicochemical characterizations

(a) *Chemical analysis*. Results concerning chemical analysis are reported in Table 1, where chemical formulae are also indicated as deduced from analysis. Elements (Al, Ba and Mn) were analyzed by atomic absorption spectroscopy after having dissolved solid in a mixture of concentrated acids (HF+HCl+$HNO_3$).

(b) *X-ray diffraction*. X-ray diffraction (XRD) has been used to identify the crystallographic phases and

Table 1
Chemical composition

| Catalyst | Ba (wt.%) | | Al (wt.%) | | Mn (wt.%) | | Fe (wt.%) | | Theoretical formula |
|---|---|---|---|---|---|---|---|---|---|
| | Theoretical | Experimental | Theoretical | Experimental | Theoretical | Experimental | Theoretical | Experimental | |
| $BaO{\cdot}6Al_2O_3$ | 17.9 | 15.84 | 42.3 | 40.35 | | | – | | $BaAl_{13}O_{20.5}$ |
| $BaFeAl_{11}O_{19}$ | 17.3 | 16.79 | 37.3 | 37.10 | – | – | 7.15 | 6.52 | $BaFe_{0.95}Al_{11.25}O_{19.22}$ |
| $BaFe_2Al_{10}O_{19}$ | 16.7 | 15.53 | 32.8 | 31.15 | – | – | 13.8 | 12.46 | $BaFe_{1.97}Al_{10.20}O_{19}$ |
| $BaFe_3Al_9O_{19}$ | 16.1 | 14.68 | 28.5 | 27.7 | – | – | 20 | 18.15 | $BaFe_{3.03}Al_{9.6}O_{19}$ |
| $BaFe_4Al_8O_{19}$ | 15.6 | 15.16 | 24.3 | 25.20 | – | – | 25.9 | 24.29 | $BaFe_{3.94}Al_{8.46}O_{19}$ |
| $BaMnAl_{11}O_{19}$ | 17.3 | 17.3 | 38.3 | 37.5 | 6.9 | 6.7 | – | – | $BaMn_{0.97}Al_{11}O_{19}$ |
| $BaMn_2Al_{10}O_{19}$ | 16.7 | 14.52 | 32.9 | 33.38 | 13.4 | 11.70 | – | – | $BaMn_{1.9}AlO_{19}$ |
| $BaMn_3Al_9O_{19}$ | 16.1 | 15.78 | 28.5 | 31.39 | 19.4 | 17.05 | – | – | $BaMn_{2.7}AlO_{19}$ |
| $BaMn_4Al_8O_{19}$ | 15.6 | 15.65 | 24.5 | 24.6 | 25.0 | 25.0 | – | – | $BaMn_4AlO_{19}$ |
| $BaFeMnAl_{10}O_{19}$ | 16.7 | 17.1 | 35.3 | 39.6 | 7.2 | 7.7 | 7.3 | 7.8 | $BaFe_{1.12}Mn_{1.12}Al_{11.8}O_{19}$ |
| $BaFeMn_2Al_9O_{19}$ | 16.1 | 16.0 | 28.6 | 30.1 | 12.9 | 13.1 | 6.6 | 6.1 | $BaFe_{0.94}Mn_{2.05}Al_{9.57}O_{19}$ |
| $BaFeMn_3Al_8O_{19}$ | 15.6 | 14.4 | 24.6 | 26.0 | 18.8 | 18.5 | 6.4 | 6.3 | $BaFe_{1.12}Mn_{3.20}Al_{8.45}O_{19}$ |

to calculate the unit cell parameters. In order to avoid any shift of the diffraction peak position, all samples were checked with an internal standard, crushed and sieved silicon powder being the standard. Data were processed, compared with the ICDD files, and plane distances along with unit cell parameters were calculated by the least squares method using the positions of 24 peaks.

(c) *BET area*. Specific surface area (SSA) was measured by using a dedicated fully computerized laboratory made BET apparatus. BET areas were calculated by using 6–7 points of nitrogen adsorption at 77 K. The solids were outgassed at 500°C for 2 h before the BET measurement.

(d) *TPR measurements*. Temperature programmed reductions (TPRs) by hydrogen were performed according to the following procedure. A known amount (50–60 mg) of sample was put in an U-shaped quartz reactor and pre-treated in air up to 400°C for 1 h at a rate of 5°C/min, then cooled down to room temperature in an argon flow. Then a mixture of 1 vol.% $H_2$ in Ar was admitted onto the samples and temperature was raised at a rate of 8°C/min up to 1000°C and maintained for 1 h at that temperature. Hydrogen consumption was deduced from the TPR profile within an accuracy of 6–8%.

(e) *Diffuse reflectance spectroscopy*. Valence state of manganese and iron ion was monitored by UV–Visible diffuse reflectance spectroscopy (DRS) using a PE Lambda 9 spectrometer equipped with an integrating sphere. Spectra were recorded at room temperature from 200 to 2500 nm using $BaSO_4$ as reference.

(f) *Mössbauer spectroscopy*. For iron containing solids, oxidation state along with local symmetry were deduced from Mössbauer spectroscopy. The spectrometer used a source of $^{57}$Co γ emitter radioisotope inserted in a rhodium matrix [13]. The latter was accelerated at constant rate, twice in a period for which the speed was inverted. Samples, diluted into pure α-alumina in order to avoid too strong absorption, were shaped into a cylindrical pellet of 16 mm in diameter. Reference used here was polycrystalline α Fe.

## 4. Catalytic activity measurements

The catalytic activity of the different solids was measured in the combustion of methane. Moreover, in order to check their thermal resistance, the catalysts were submitted to an accelerated aging. Differences between catalytic properties of as-prepared solids and aged ones associated with further physicochemical characterizations allowed to classify the catalysts according to their thermal stability. Experimental conditions were as follows:

- *Catalytic activity*. Mass of catalyst: 500 mg; pre-treatment: $O_2$ at 400°C for 1 h; reactants mixture: 4 vol.% $O_2$ and 1 vol.% $CH_4$ in nitrogen as balance; total flow rate=6.4 l $h^{-1}$ corresponding to a GHSV of 15 000–25 000 $h^{-1}$.
- *Aging procedure*. 1200°C; 24 h with 3 g of catalyst: $O_2$+$H_2O$+$N_2$ mixture (5 vol.%+6 vol.%+89 vol.%); 10 l $h^{-1}$.

## 5. Results

(a) *Chemical analysis*. After calcination at 1200°C, the acidic attack is difficult and may lead to false values in the case of incomplete dissolution. The results reported in Table 1 showed that, in every case, the M/Ba and M/Al experimental ratios are very close to the theoretical ones. Since oxygen has never been analyzed, formulae reported here are right as far as oxygen stoichiometric ratios are not considered.

(b) *Structure of reference matrix*. Structure of $BaAl_{12}O_{19}$ was only obtained after calcination at 1200°C with an SSA of 11 $m^2$/g. However, very small amounts of barium aluminate $BaAl_2O_4$ were observed by XRD. The barium aluminate phase is no longer observed after a subsequent air calcination at 1300°C during 24 h, the only phase observed here was the hexaaluminate one with an SSA of 7 $m^2$/g. However, the structure experimentally observed is always that referred in the ICDD files as $BaO{\cdot}6.6Al_2O_3$. According to the stoichiometric Ba/Al=6 ratio of the initial alkoxides, this would correspond to a structure where BaO should be in excess outside, and according to the temperature of calcination, should not escape the X-ray analysis. In fact according to previous studies, there is a broad range of composition for β-$Al_2O_3$ which will be discussed further (*vide infra*).

(c) *Structure of iron containing solids*. XRD spectra also evidenced the $BaAl_{13.2}O_{21.8}$ ($BaO{\cdot}6.6Al_2O_3$) structure. Some very small amounts of α-$Al_2O_3$ were sometimes detected. However, a few weak peaks were

ascribed to the presence of another phase namely $BaAl_{12}O_{19}$ ($BaO{\cdot}6Al_2O_3$). In fact, the two hexaaluminate structures are identical and correspond to slight difference of aluminum concentrations (see thereafter). Calculations of unit cell parameters were done essentially on the *a* parameter because it is most affected by the introduction of foreign cations.

For the fresh catalysts, the introduction of increasing amounts of $Fe^{3+}$ cations inside the bulk leads to an increase of both *a* and *c* parameters. For the *a* parameter the increase is strongly evidenced for the first cation introduced, then it increases slowly and smoothly. A more regular increase is observed for the *c* parameter since an almost linear increase with the iron loading is observed. For aged solids, no simple trends of both *a* and *c* parameters could be deduced. Nevertheless, a global increase of the values of both parameters with the iron content was observed.

Mössbauer spectroscopy analysis showed that iron ions are substituting aluminum as only $Fe^{3+}$ since $Fe^{2+}$ ions are not detected. Moreover, only octahedral sites are occupied by iron and tetrahedral sites are free of $Fe^{3+}$ species.

In conclusion, the introduction of $Fe^{3+}$ cations bulkier than the $Al^{3+}$ ones leads to a slight expansion of the unit cell volume. Until 4 $Fe^{3+}$ ions per unit cell, the hexaaluminate structure is preserved and there is non-iron species outside of the matrix.

(d) *Structure of manganese containing solids*. In the case of the solids containing 1, 2 or 3 $Mn^{3+}$ ions per unit cell and calcined under oxygen at 1200°C only the β-$Al_2O_3$ structure was observed, and no intermediate barium aluminate was detected contrary to the non-substituted matrix.

The three solids gave diffraction patterns identical to that of the support. Only the position of diffraction peaks were shifted, the larger the Mn content, the higher the shift. Like for iron containing solids, the variation of the *a* parameter increases almost linearly with the number of foreign cations from 0 to 3. When aged, the three solids do not show any significant modification of their *a* parameter. The same is not true for *c* because the solids expand only moderately in *c* as the manganese loading increases in either fresh or aged states: variations of *c* are not very relevant here.

For the $BaMn_4Al_8O_{19}$ solid, Mn was not fully incorporated in the hexaaluminate structure and the sample is polyphased. Besides the regular hexaaluminate structure, some other phases were detected like BaO, $Al_2O_3$ and $Mn_2O_3$ and the extra peaks are rather large. This means that substitution of Mn inside the hexaaluminate structure is limited, or that the reaction is not complete for kinetics reasons.

(e) *Structure of solids containing both iron and manganese*: $BaFeMn_xAl_{1-x}O_{19}$. The mixed solids have been prepared with a substitution level of 1 $Fe^{3+}$ ion per unit cell and variable amount of manganese. The three solids containing up to 4 cations seem to behave like those containing only manganese. Up to 3 cations per unit cell (1 Fe+2 Mn), only one phase is observed which is that corresponding to $BaAl_{13.2}O_{20.8}$. Very minute amounts of the other hexaaluminate $BaAl_{12}O_{19}$ along with traces of α-alumina, $BaAl_2O_4$ and another phase related to the spinel structure are detected. However, for the solid $BaFeMn_3Al_8O_{19}$ at least two phases are evidenced, the hexaaluminate structures and the spinel one.

The evolution of the unit cell parameters is similar to that observed for only manganese containing solids: *c* does not change very much whereas *a* increases almost linearly up to 3 cations per unit cell (1 Fe+2 Mn) leading to a global 1.55% of expansion, the same value as for solid containing 3 Mn per unit cell. However, for the last solid which is not homogeneous, calculations indicate clearly that there is a sharp decrease for *a* and an increase for *c* (Table 2).

Mössbauer spectroscopy measurements show the same trend as for solids containing only iron: only $Fe^{3+}$ ions occupying octahedral sites are detected. The presence of manganese ions does not strongly modify the valence state and the location of iron.

(f) *Specific surface areas*. BET areas of fresh and aged substituted hexaaluminates are reported in Table 3. Introduction of foreign cations does lead to a loss of the thermal stability. On the contrary and as far as Mn-substituted hexaaluminates are concerned, the SSA values are larger than that of the parent barium hexaaluminate. After aging, the substitution by manganese does not induce extra sintering. The same is also true for iron but to a lower extent.

(g) *Diffuse reflectance spectroscopy*. The solids containing 1–3 Mn ions per unit cell show essentially the same spectrum which is typical of the $MnO_6$ chromophore (Fig. 1). Two bands at 250 and 450 nm are observed. The 250 nm band is relatively intense and should correspond to a charge transfer between

Table 2
Crystallographic phases observed by XRD, BET areas and unit cell parameters[a]

| Catalyst | XRD of fresh state | XRD of aged state | BET area ($m^2$/g) (F–A) | Unit cell parameter *a* (Å) (F-A) | Unit cell parameter *c* (Å) (F–A) |
|---|---|---|---|---|---|
| $BaO{\cdot}6\ Al_2O_3$ | $HA_I$+BA | $HA_I$+$HA_{II}$ | 11–9 | 5.586 (F) | 22.725 (F) |
| $BaFeAl_{11}O_{19}$ | $HA_I$+$HA_{II}$+AA | $HA_I$+$HA_{II}$+AA | 14–12 | 5.609–5.600 | 22.746–22.778 |
| $BaFe_2Al_{10}O_{19}$ | $HA_I$+$HA_{II}$+AA | $HA_I$+$HA_{II}$+AA | 12–9 | 5.612–5.599 | 22.748–22.818 |
| $BaFe_3Al_9O_{19}$ | $HA_I$+$HA_{II}$+AA | $HA_I$+$HA_{II}$+AA | 10–7 | 5.612–5.627 | 22.755–22.753 |
| $BaFe_4Al_8O_{19}$ | $HA_I$+$HA_{II}$+AA | $HA_I$+$HA_{II}$+AA | 6–5 | 5.613–5.613 | 22.778–22.682 |
| $BaMnAl_{11}O_{19}$ | $HA_I$+AA | $HA_I$+ AA | 20–15 | 5.625–5.625 | 22.761–22.761 |
| $BaMn_2Al_{10}O_{19}$ | $HA_I$+BA+AA | $HA_I$+BA+AA | 14–11 | 5.647–5.647 | – |
| $BaMn_3Al_9O_{19}$ | $HA_I$ | $HA_I$ | 14–9 | 5.661–5.661 | – |
| $BaMn_4Al_8O_{19}$ | $HA_I$+BA+$Mn_2O_3$ | $HA_I$+BA+$Mn_2O_3$ | 10–6 | 5.674–5.674 | – |
| $BaFeMnAl_{10}O_{19}$ | $HA_I$+$HA_{II}$+AA | $HA_I$+$HA_{II}$+AA | 15–11 | 5.652–5.657 | 22.560–22.861 |
| $BaFeMn_2Al_9O_{19}$ | $HA_I$+$HA_{II}$+AA+BA+SP | $HA_I$+$HA_{II}$+AA+BA+SP | 11–9 | 5.675–5.672 | 22.846–22.821 |
| $BaFeMn_3Al_8O_{19}$ | $HA_I$+$HA_{II}$+SP | $HA_I$+$HA_{II}$+SP | 7–4 | 5.629–5.678 | 23.734–22.848 |

[a] $HA_I$ and $HA_{II}$ stand for hexaaluminate $BaAl_{13.2}O_{20.8}$ and $BaAl_{12}O_{19}$; BA, AA and SP stand for barium aluminate $BaAl_2O_4$, $\alpha$-$Al_2O_3$ and spinel, respectively; $\alpha$-$Al_2O_3$ peaks are always very weak; F and A stand for fresh and aged.

oxygen anion and manganese cation because no d–d transitions are possible at such energies for the first series of transition metal ions. The band at 450 nm, of lower intensity, is related to $Mn^{x+}$ ions. Considering the numerous oxidation states of manganese (+2, +3, +4, +6, +7), only the 3+1 leads to a spectrum consisting of a single band at ca. 450–500 nm [14] for oxygenated ligand giving the $MnO_6$ chromophore. It is related to the unique spin-allowed d–d transition for a $d^4$ electronic configuration in an octahedral field. Thus DRS confirms without ambiguity that manganese does enter the hexaaluminate network and that both symmetry and oxidation state are relevant to $Mn^{+3}$. However, the band intensity is not truly proportional to the number of introduced cations.

For solids containing iron only, DRS is of little help because no features are observed. All solids are light-brown and show a strong charge transfer at 250 nm whose intensity is almost constant. However, no absorption is observed in the near infrared range. This is another clue that ferrous ions are unlikely. In the presence of $Fe^{2+}$ ions, some characteristic bands should have been observed.

For the solids containing both kinds of ions, absorptions of $Mn^{3+}$ and $Fe^{3+}$ ions are superimposed that make the spectra difficult to interpret. The charge transfer of $Fe^{3+}$ (or $Mn^{3+}$) is still present at 250 nm, a strong shoulder at 450 nm is still observed due to manganese ions and no absorption is observed in the near infrared. Thus, trivalent ions are observed by this technique.

(h) *TPR experiments*. The TPR profiles concerning the reduction of fresh $BaFe_xAl_{12-x}O_{19}$ are given in Fig. 2 and are characterized by two reduction zones. The reduction starts at 300–350°C suggesting a reducibility behavior independent on the Fe content. Then there is a first maximum at 570°C for $x$=1 or 2 which shifted to 710°C for $x$=3 or 4. A second maximum appears at 950°C, whatever be the iron concentration in the solid and its intensity increases with the

Table 3
TPR values: number of M (Mn and/or Fe) ions reduced at $\theta_1$=500°C and at $\theta_2$=1000°C[a]

| | $BaFe_1$ | $BaFe_2$ | $BaFe_3$ | $BaFe_4$ | $BaMn_1$ | $BaMn_2$ | $BaMn_3$ | $BaMn_4$ | $BaFeMn_1$ | $BaFeMn_2$ | $BaFeMn_3$ |
|---|---|---|---|---|---|---|---|---|---|---|---|
| $\theta_1$ | 0.15 | 0.42 | 0.29 | 0.23 | 0.055 | 0.28 | 0.32 | 0.36 | 0.35 | 0.29 | 0.40 |
| $\theta_2$ | 0.78 | 0.2 | 1.4 | 3.2 | 0.21 | 1.20 | 3 | 2.9 | 1.5 | 1.97 | 3.2 |

[a] At $\theta_1$=500°C only the reduction of $M^{3+}$ to $M^{2+}$is assumed ($Mn^{2+}$ or $Fe^{2+}$); at $\theta_2$=1000°C, the reduction of $Fe^{2+}$ into $Fe^0$ is assumed, whereas the $Mn^{2+}$ ions are not affected.

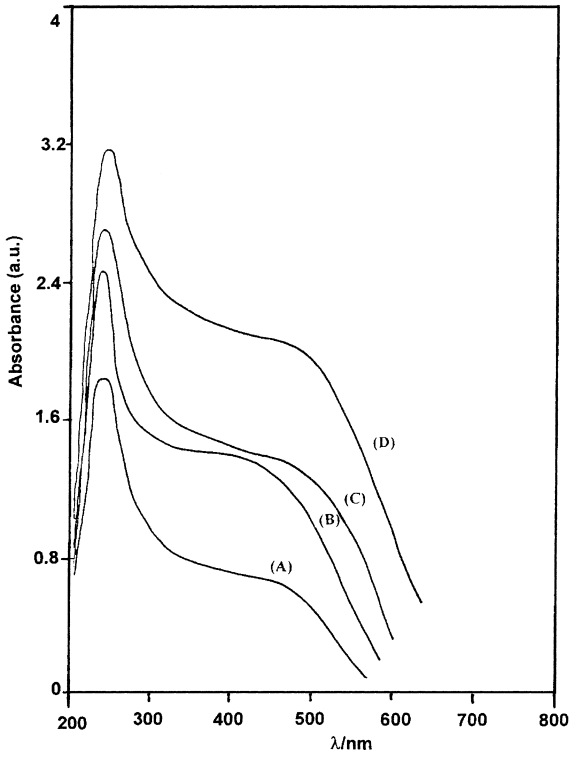


Fig. 1. Diffuse reflectance spectra of $BaMn_xAl_{12-x}O_{19}$ catalysts: (A) $x$=1, (B) $x$=2, (C) $x$=3 and (D) $x$=4.

iron loading. During the plateau at 1000°C, a continuous consumption of hydrogen is observed and it increases with the amount of iron. Hydrogen consumption according to the temperature has been calculated for the four samples but due to the shape of the profiles, values are not fully reliable. This is easy to perform for the $BaFe_1Al_{11}O_{19}$ sample, and difficult or almost impossible for the other three samples. The first reduction peak has been ascribed to $Fe^{2+}$ formation and at 1000°C a total reduction into $Fe^0$ has been assumed. The number of $Fe^{3+}$ ions reduced at 500°C has been calculated and the catalytic activities have also been calculated at that temperature.

For $BaMn_xAl_{12-x}O_{19}$ (Fig. 3) the reduction was expected to be limited to $Mn^{2+}$ ions formation because $Mn^{2+}$ species are not reducible even at 1000°C. It seems that two species are present, one being reduced near 600°C, whereas the reduction of the second one starts at 800°C and has a maximum at 1000°C. The numbers of reduced ions has been calculated at 500 and at 800°C. The $BaMn_1Al_{12}O_{19}$ solid is poorly reducible because 21% of Mn is reduced at 1000°C, 5.5% before 800°C and only 4% at 500°C (Table 3). The non-reducibility may be accounted for the presence of $Mn^{2+}$ ions escaping analysis. Cations of high valence are not stable at high

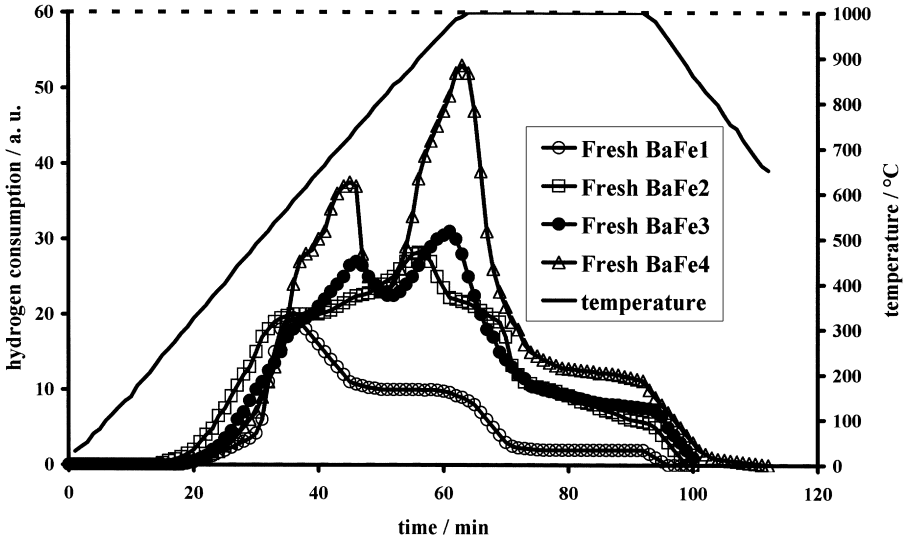


Fig. 2. TPR under hydrogen of fresh $BaFe_xAl_{12-x}O_{19}$ catalysts.

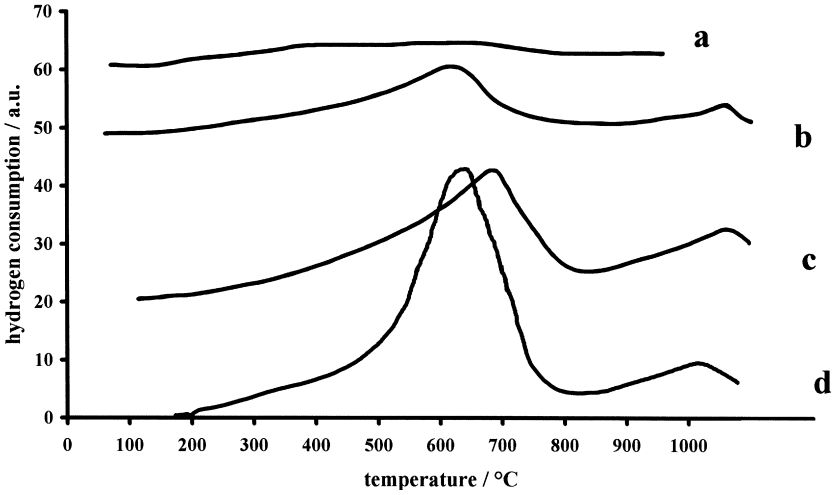


Fig. 3. TPR under hydrogen of fresh $BaMn_xAl_{12-x}O_{19}$catalysts: (a) $x$=1, (b) $x$=2, (c) $x$=3 and (d) $x$=4.

temperature: this is true for the +4, +6 and +7 oxidation states of manganese. The only oxidation state that can be present is $Mn^{2+}$, which is non-detectable by DRS due to spin-forbidden transitions of very low intensities. Rather intense $Mn^{3+}$ d–d transitions completely obscure the eventual presence of $Mn^{2+}$ transitions. When octahedrally coordinated, and with a high spin state as is usual, the species has a radius of 0.87 Å, which should induce a lot of stress due to non-matching of both charge and radius. Thus, it is postulated that for $BaMn_1Al_{12}O_{19}$ solid, Mn enters the structure essentially as divalent cation.

For the other two solids ($BaMn_2$ and $BaMn_3$), the number of Mn ions reduced per unit cell before 500°C is almost the same (0.28 and 0.32). Calculation for reduction up to 1000°C leads to values of 1.21 and 3, respectively. Thus when manganese ions are introduced into hexaaluminate, the fraction of reducible ions increases with manganese content. One conclusion deduced from the TPR results is that the higher the Mn content introduced into the hexaaluminate structure, the larger is the $Mn^{3+}$ cation concentration. Finally, in $BaMn_3Al_8O_{19}$, which can be totally reduced, manganese is exclusively present as $Mn^{3+}$ octahedrally coordinated ions.

A TPR study has been also performed on fresh $BaFeMn_xAl_{11-x}O_{19}$ (Fig. 4). Generally speaking, the hydrogen consumption increases with the manganese loading. But the catalysts contain 2 cations of different reducibility. For solids containing 1 or 2 Mn ions per unit cell, TPR profiles are almost similar, meaning same cation properties. A first sharp peak is observed at 485°C ($BaFeMnAl_{10}O_{19}$) or at 435°C ($BaFeMn_2Al_9O_{19}$) and a wide one whose maximum is located at 925 or 1000°C. It is important to note that the temperature corresponding to the peaks for $BaMn_xAl_{12-x}O_{19}$ and located in the 600–700°C range is now not observable. But it does appear for the last sample $BaFeMn_3Al_8O_{19}$, meaning a different behavior as long as manganese reducibility is considered. The number of ions reduced into $M^{2+}$ is given in Table 3 which shows also that the total reduction of iron is never achieved: maximum looks like those corresponding to solids containing manganese alone.

## 6. Catalytic activity measurements

The fresh and aged solids were tested in the catalytic combustion of methane (Figs. 5–7) and a general increase in the catalytic activity when increasing the amount of active cations is observed. However, some differences appear due to variations of surface areas.

The matrix itself is not inactive since conversions of 10 and 20% are observed at 700 and 750°C, respectively, a full conversion is obtained near 800°C. The $T_{10}$, $T_{50}$ and $T_{90}$ temperatures corresponding to 10, 50 and 90% conversion are reported in Table 4

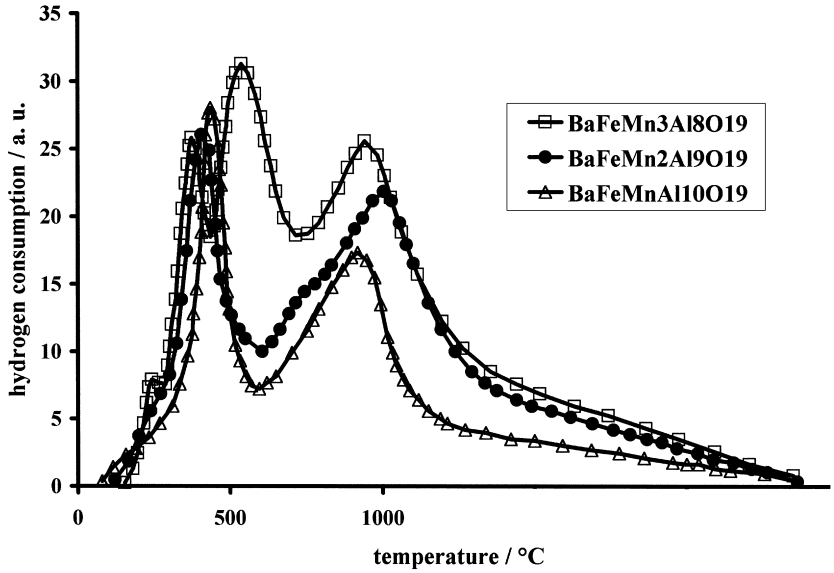


Fig. 4. TPR under hydrogen of fresh $BaFeMn_xAl_{11-x}O_{19}$ catalysts.

for fresh and aged catalysts. The $BaMn_3Al_9O_{19}$ solid in the aged state is more active than the fresh solid containing only 1 Mn per unit cell. The same is also observed for iron substituted hexaaluminates, where the introduction of 2 $Fe^{3+}$ ions per unit cell leads to a solid which is more active in the aged state than the fresh $BaFe_4Al_8O_{19}$. For catalysts containing both cations, $BaFeMnAl_{10}O_{19}$ is practically equivalent to $BaMn_3Al_9O_{19}$, either in fresh state or in aged one (Table 4).

The intrinsic activities of the various catalysts (mol $CH_4$ converted per hour and per square meter) are given in Figs. 8–11. When compared to the barium hexaaluminate parent, the introduction of

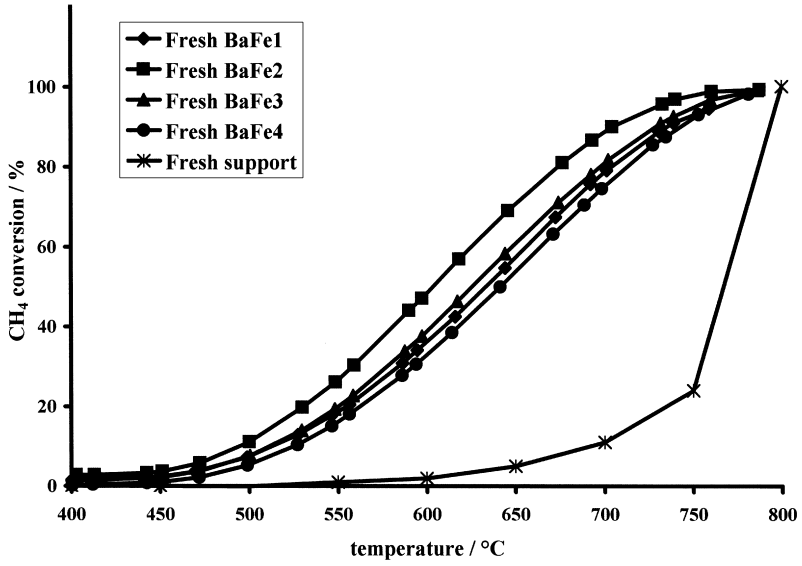


Fig. 5. Catalytic combustion of $CH_4$ over fresh $BaFe_xAl_{12-x}O_{19}$ catalysts.

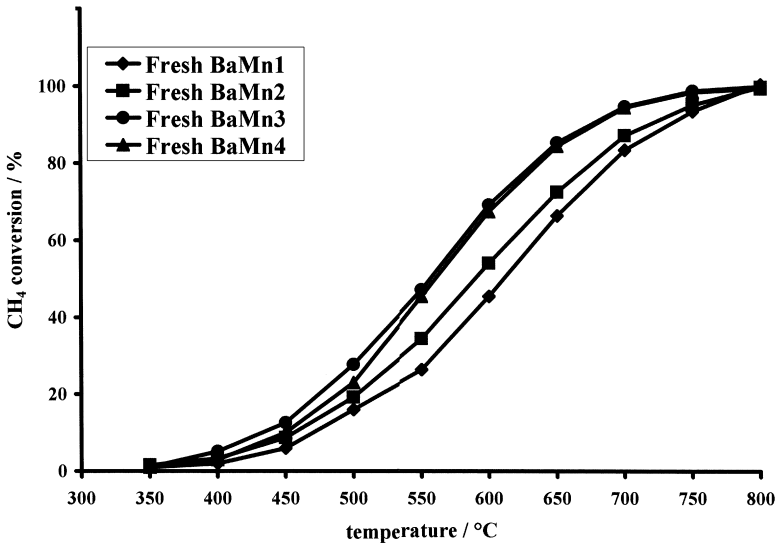


Fig. 6. Catalytic combustion of $CH_4$ over fresh $BaMn_xAl_{12-x}O_{19}$ catalysts.

active cations, like iron or manganese, enhances the activity by ca. two orders of magnitude. Table 4 shows this behavior and indicates also that activities are roughly similar whatever be the nature of the cation, provided substitution levels are identical. However, there is a global increase of intrinsic activity with cation loading. Nevertheless, there is no linear relationship and the cations firstly introduced seem to be more efficient. For the solids containing both iron and manganese, the additivity of the activities seems only valuable for the low substitution levels.

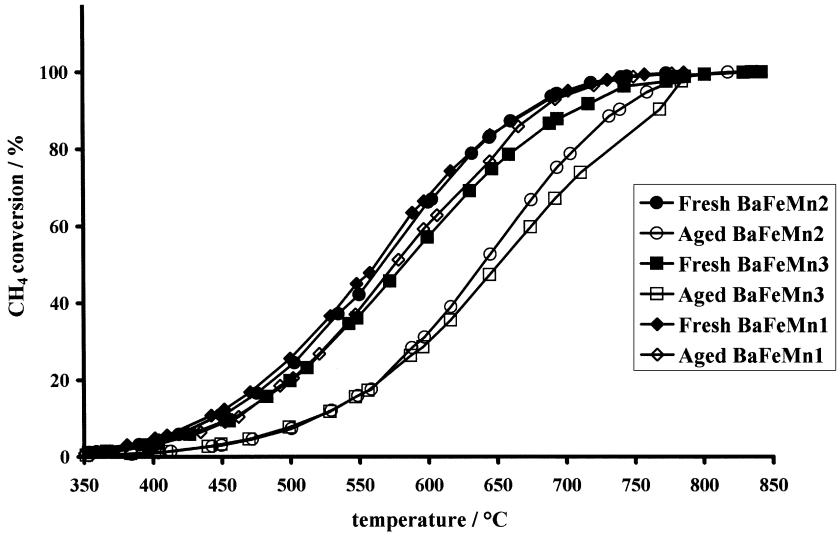


Fig. 7. Catalytic combustion of $CH_4$ over fresh and aged $BaFeMn_xAl_{11-x}O_{19}$ catalysts.

Table 4
Catalytic activity expressed as $T_{10}$, $T_{50}$ and $T_{90}$ in °C and as intrinsic activity ($10^{-5}$ mol $CH_4$ converted per hour and per square meter) for both fresh (F) and aged (A) solids

| Solid | $T_{10}$ (F–A) | $T_{50}$ (F–A) | $T_{90}$ (F–A) | $E_a$ (kJ mol$^{-1}$) (F–A) | Intrinsic activity at 500°C |
|---|---|---|---|---|---|
| $BaAl_{12}O_{19}$ | 700 (F) | ≈770 (F) | ≈800 (F) | n.a. | 0.035 |
| $BaFeAl_{11}O_{19}$ | 515–545 | 635–665 | 740–760 | 92–95 | 2.8 |
| $BaFe_2Al_{10}O_{19}$ | *495–520* | *605–640* | *705–755* | 79–100 | 4.7 |
| $BaFe_3Al_9O_{19}$ | 510–540 | 625–665 | 730–760 | 85–91 | 5.1 |
| $BaFe_4Al_8O_{19}$ | 520–540 | 640–705 | 745–775 | 86–110 | 6.4 |
| $BaMnAl_{11}O_{12}$ | 470–575 | 610–700 | 730–800 | – | 2.5 |
| $BaMn_2Al_{10}O_{19}$ | 460–470 | 590–610 | 720–760 | – | 4.4 |
| $BaMn_3Al_9O_{19}$ | *425–460* | *560–590* | *670–700* | – | 6.0 |
| $BaMn_4Al_8O_{19}$ | 440–495 | 555–605 | 680–730 | – | 6.6 |
| $BaFeMnAl_{10}O_{19}$ | *440–460* | *560–570* | *675–710* | 80–85 | 5.0 |
| $BaFeMn_2Al_9O_{19}$ | 440–520 | 565–640 | 670–740 | 85–85 | 6.2 |
| $BaFeMn_3Al_8O_{19}$ | 460–515 | 580–650 | 705–770 | 80–80 | 8.0 |

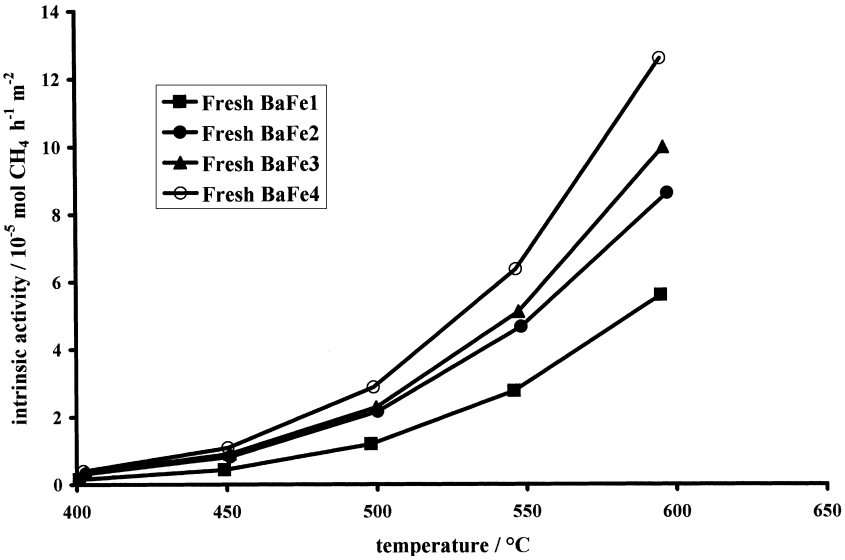


Fig. 8. Intrinsic activity of fresh $BaFe_xAl_{12-x}O_{19}$ catalysts.

## 7. Discussion

### 7.1. Structure

It is clear that the sol–gel method previously described by Arai and co-workers [12] is very worthwhile for preparing substituted hexaaluminates. However, the structure experimentally observed is always referred in the ICDD files as $BaO{\cdot}6.6Al_2O_3$. According to the stoichiometric Ba/Al=6 ratio of the initial alkoxides, this would correspond to a structure where BaO should be in excess outside, and according to the temperature of calcination should not escape the X-ray analysis. Previous studies have shown the existence of a broad range of composition for β-$Al_2O_3$, and two main structures seem to exist [15]. One noted β or phase I corresponds to $0.9BaO, 6Al_2O_3$ (alumina-rich phase), whereas the other noted β′, or phase II corres-

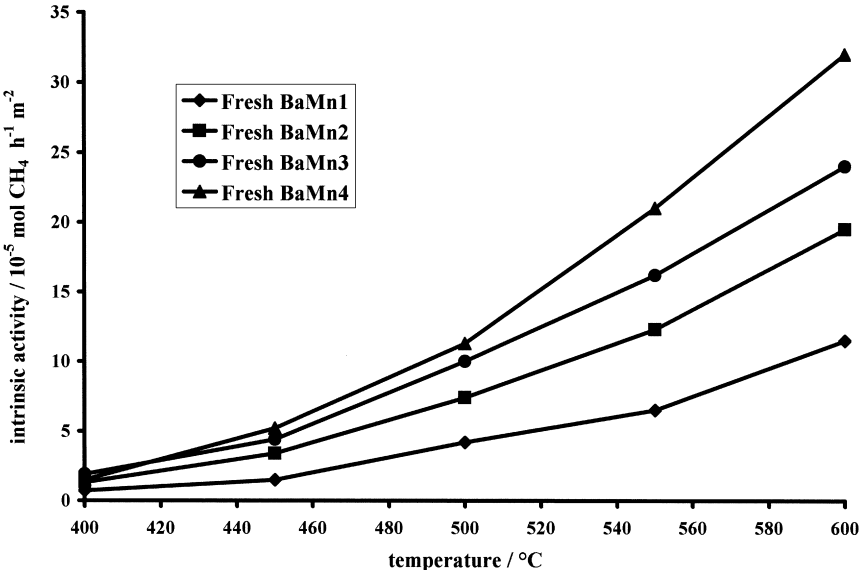


Fig. 9. Intrinsic activity of fresh $BaMn_xAl_{12-x}O_{19}$ catalysts.

ponds to $1.3BaO, 6Al_2O_3$ (alumina-poor phase). Thus in our case the solid may correspond to a solid solution of 30 mol% of β′ into 70% of β or to a mixture of both phases: only the latter β′, being predominant, is detected by XRD. α-alumina was never detected. Similar experiments performed with γ-alumina have shown that the corindon phase is the only structure obtained at 1200°C with an SSA of $4\,m^2/g$ [16]. In the present study, only traces of $\alpha$-$Al_2O_3$ were sometimes observed.

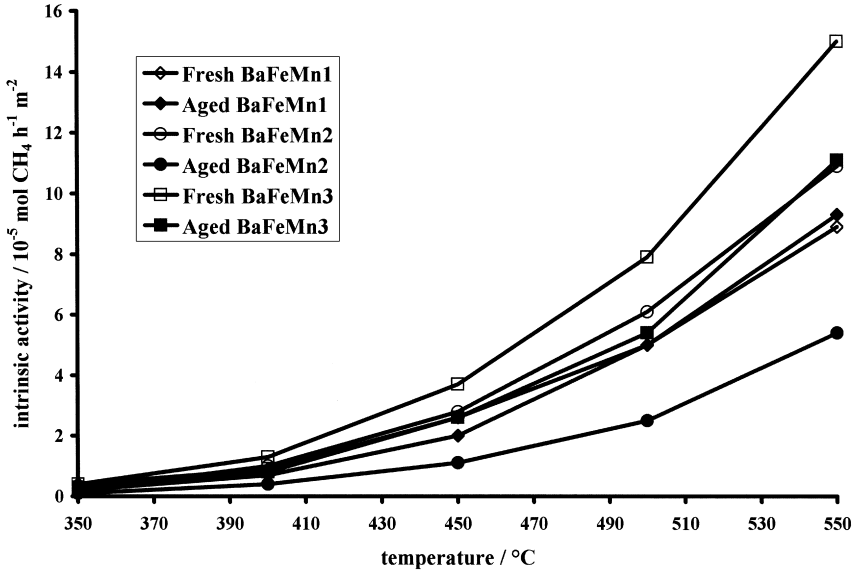


Fig. 10. Intrinsic activity of $BaFeMn_xAl_{11-x}O_{19}$ catalysts.

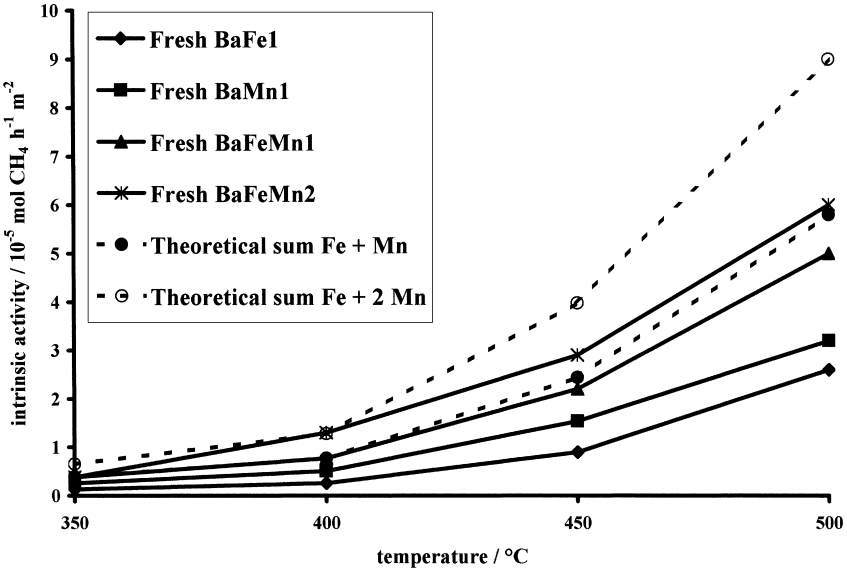


Fig. 11. Intrinsic activities of $BaM_xAl_{12-x}O_{19}$ catalysts. Comparison between solids containing 1 Fe, 1 Mn, 1 Fe+1 Mn and 1 Fe+2 Mn per unit cell. Broken lines correspond to theoretical values corresponding to the sum of the activities of the corresponding monosubstituted hexaaluminates.

The unit cell parameters (Table 2) calculated for the support after calcination at 1200°C are identical to those obtained by Arai et al. Moreover, the *a* and *c* values correspond quite well with that recently reported by Groppi et al. [17] for $BaMn_1Al_{12}O_{19}$ for which the magnetoplombite structure is referred with *a*=5.594 Å and *c*=22.76 Å. Recently also Kutty and Nayak [18] noted that *a* parameter slightly decreased with increasing Ba/Al ratio (from 1/7.4 to 1/4.5) and should have a value of 5.60 for Ba/Al=1/6.6, whereas *c* increased much more rapidly from 22.78 to 22.95 Å and should have a value of 22.78 Å close to the value found in the present work (22.74 Å).

Almost pure single phased solids are obtained. Only in two cases the XRD diagrams reveal the presence of large amounts of another phase: solids expected to contain 4 Mn or 3 Mn+1 Fe ions per unit cell (see Table 2). Thus hexaaluminate structure can accommodate 3 cations (either $Fe^{3+}$ or $Mn^{3+}$) without segregation and can tolerate eventually 4 $Fe^{3+}$ ions. When manganese is present, stress seems to be more intense.

Introduction of foreign bulkier cation leads to an expansion of unit cell because both $Fe^{3+}$ and $Mn^{3+}$ cations are larger than the $Al^{3+}$ ones. Due to the structure of hexaaluminate consisting of aluminum spinel layers separated by BaO planes, incorporation of cations can occur in tetrahedral or octahedral sites of oxygen close packing, aluminum ions occupying both types of sites. In addition, $Fe^{3+}$ substitution leads to changes in the *a* parameters which are more important than for the *c* parameter. The same phenomenon is observed for manganese for which the modifications of the *a* values are more pronounced. This behavior is connected with the radii values of the 3 cations.

In octahedral symmetry, the radii of $Al^{3+}$, $Fe^{3+}$ and $Mn^{3+}$ ions are 0.53, 0.65 and 0.65 Å, respectively [19,20]. Tetrahedral symmetry values are 0.39 and 0.49 Å for aluminum and iron ions, respectively ($Mn^{3+}$ ion does exist in tetrahedral symmetry). Thus introduction of $Fe^{3+}$ ($Mn^{3+}$) increases the M–O distance for the $MO_6$ chromophore. On the other hand if $Fe^{3+}$ ions enter tetrahedral sites, expansion of bond distances should be much more pronounced. For iron containing hexaaluminate, expansions of unit cell parameters for *a* and *c* are limited to a maximum of 0.48 and 0.23%, respectively (when solid contains 4 cations per unit cell). For solids containing manganese, expansion of *a* is equal to 1.56% for the solid containing 4 ions Mn per unit cell. For solids containing 1 Fe and 2 Mn (3 cations), expansion of *a* parameter is

also as high as 0.87%. Thus, despite identical radii, introduction of manganese causes much more stress, that is evidenced for the solid $BaMn_4Al_8O_{19}$, in which extra-phases are present.

Effect of manganese is too important and another cause should be found to explain this particularly important effect of aging. The latter must be another valence state of manganese. When considering TPR of the four fresh solids containing manganese only, some intriguing results are obtained.

The total reduction percentage is not 100% except for the $BaMn_3Al_9O_{19}$. On the contrary, the $BaMnAl_{11}O_{19}$ seems to be non-reducible because only 21% of Mn is transformed into Mn(II) state. This is not consistent with the exclusive presence of $Mn^{3+}$. On the contrary, if $Mn^{2+}$ ions present in the precursor enter a position in the aluminate network, they may survive during the calcination step and may not be oxidized into $Mn^{3+}$. But $Mn^{2+}$ is larger and should expand the unit cell too much, as experimentally observed. For 1, 2, 3 or even 4 introduced cations, expansion is more important for Mn than for Fe. In conclusion substituting Al by Mn leads to a solid containing both $Mn^{2+}$ and $Mn^{3+}$ ions. DRS study also showed that increasing the metal loading leads to an increase of absorption due to $Mn^{3+}$. Cations introduced first enter the hexaaluminate structure as $Mn^{2+}$ ions probably forming locally the $MnAl_2O_4$ spinel. Increase of the Mn loading may lead to more $Mn^{3+}$ species in place of $Al^{3+}$ in the hexaaluminate structure.

The case of the substitution by iron is more simple because iron enters the network only as $Fe^{3+}$ ions and $Fe^{2+}$ ions have never been observed. Such a conclusion is also confirmed by Mössbauer spectroscopy meaning that during the synthesis step, iron, which is in a trivalent state at the very beginning, does enter the hexaaluminate network as a trivalent one and that no decomposition occurs even at 1200°C. When cation concentration increases, the values of both *a* and *c* parameters increase and the distribution of $Fe^{3+}$ ions among the various types of sites is changed as previously published [21].

For two substituted barium hexaaluminates a phase segregation is observed. That is the case of solids containing 4 cations per unit cell and essentially manganese. It is quite strange that both trivalent ions ($Mn^{3+}$ and $Fe^{3+}$) having identical radii behave differently. It should be remembered that iron leads to hexaferrite structure, whereas manganese does not. So it might be concluded that manganese is only partially soluble in barium hexaaluminate contrary to iron which may be considered as totally soluble. Between $BaAl_{12}O_{19}$ and $BaFe_{12}O_{19}$, a lot of intermediate compositions with Al+Fe=12 might exist with a similar structure.

### 7.2. Activity

The support itself is not inactive even if its activity is rather weak, the value of the apparent activation energy is 95 kJ mol$^{-1}$. The activity has been explained by a parallel reaction like oxidative coupling leading to some traces of ethylene that burns instantaneously [22]. When transition metal ions are introduced substituting the aluminum ones, the activity increases along with metal concentrations. However, when comparing the behaviors of $BaMn_xAl_{12-x}O_{19}$, $BaFe_xAl_{12-x}O_{19}$ and $BaFeMn_xAl_{11-x}O_{19}$, some differences are observed, either between cations for same metal loading, or for different loadings for same cation. Values of light-off ($T_{50}$) as well as those of intrinsic activities are given in Table 4. Only 30°C separates the half conversion temperatures for fresh and aged best catalysts like $BaMn_3Al_9O_{19}$, $BaFe_2Al_{10}O_{19}$ and only 10°C for $BaFeMnAl_{10}O_{19}$. $BaFeMnAl_{10}O_{19}$ must be called thermostable catalyst, because severe aging has almost no effect on the catalytic activity, the TPR profile, the distribution of the cations in the different sites and the SSA value.

For solids containing manganese, activity also increases with the manganese content. However, in the fresh state and for equivalent substitution levels, the catalytic activities of Mn-substituted hexaaluminates are close to those of the corresponding Fe-substituted samples.

For the $BaMn_2Al_{10}O_{19}$ and $BaMn_3Al_9O_{19}$ catalysts, aging has a limited effect because light-off temperatures are only displaced by 20–30°C. In addition, the aged solid $BaMn_3Al_9O_{19}$ shows an activity higher or comparable to those of solids containing 1 or 2 $Mn^{3+}$ per unit cell. Two opposite effects occur: SSAs and transition metal ions content. So an optimum has to be observed.

For the four Fe-substituted solids, the changes in catalytic activity were not associated with changes in

the apparent activation energies. This means that irrespective of whether iron is present or not, the limiting step remains the same.

As far as conversions are concerned, the solid $BaFe_2Al_{11}O_{19}$ is the most active, and increasing the iron content is not valuable. This is partly due to BET areas that decrease almost linearly when iron content increases. A low concentration of foreign cations is beneficial for activity by increasing actives species, but at the same time some stress is produced due to the larger size of $Fe^{3+}$ ions compared to that of $Al^{3+}$ ones. If the iron concentration is too high, a too strong constrain is induced leading to a loss of area after aging. Since the active sites are located at the surface, sintering leads to a decrease of the catalytic activity. This is true for fresh and aged catalysts. The increasing number of active cations is counterbalanced by lowering the SSA.

For comparing all the solids irrespective of the different BET areas, superficial activity is much more reliable because it does not take area modifications into account. Similar results have been obtained by Groppi et al. [23] with iron doped barium hexaaluminate even if they used another method of synthesis which is the precipitation of carbonates [17].

At a given temperature, the activity increases with cation content but is not proportional to it. Thus for the solid containing 4 $Fe^{3+}$ ions per unit cell, the activity in the fresh state was only 2.4 times that corresponding to the monosubstituted sample. The same is true for aged solids. After aging, the loss in catalytic activity corresponds to the BET area loss. Thus, sintering is the only effect of aging: the number of surface active sites decreases but their nature is not modified since the intrinsic activity is not changed.

The latter class of solids is concerned with $BaFeMn_xAl_{11-x}O_{19}$. For the $BaMnFeAl_{10}O_{19}$ solid, the intrinsic activity is exactly the sum of the activities of the two monosubstituted catalysts. Thus a statistical distribution of iron and manganese is expected to occur and the formation of Fe–O–Mn species seems unlikely. On the contrary, when $x$=2 or 3 activities are not the sum of activities of $BaFeAl_{11}O_{19}$ and 2 or 3 times that of $BaMnAl_{11}O_{19}$. This means that when the cations concentration is low (1 Fe+1 Mn) each species behave independently from the other. In other words, there is the same surface trivalent ions concentration: Fe is only as $Fe^{3+}$, whereas Mn is present in two valence states $Mn^{2+}$ and $Mn^{3+}$. There is no mutual influence. However, as Mn concentration increases, it seems that some species are escaping the surface, like for $BaMn_xAl_{12-x}O_{19}$, because intrinsic activity is not fully proportional to the cation concentration. This may be connected to the TPR results showing that reducibility increases not linearly with the cation concentration. For solids containing manganese, some species are also not reducible at below 500°C. When too much manganese is inserted in the matrix, the number of surface active species is reduced. Other structural studies are necessary for elucidating real positions of each cation in the bulk and possibly on the surface.

## 8. Conclusion

Synthesis of barium hexaaluminate via metal alkoxides hydrolysis is an efficient method for obtaining pure single phased solids with a rather well-developed SSA. Introduction of $M^{n+}$ ions during the hydrolysis step leads to a gel very homogeneous in Ba, M and Al. Further calcination at 1200°C leads to the exactly desired structure. Substitution of aluminum by iron or manganese ions, having the same charge (+3), the same local symmetry ($O_h$) and comparable radius, is possible at least for 3 ions per unit cell. Introduction of a fourth Mn ion is not allowed because of an increasing constraint which destabilizes the structure. Part of manganese is present as $Mn_2O_3$ which is outside the hexaaluminate structure. Concerning the valence state of ions introduced, it seems that both $Mn^{+2}$ and $Mn^{+3}$ are present, and the lower the manganese concentration, the higher the $Mn^{2+}$ content. Only one kind of Mn ion ($Mn^{3+}$) seems to be present in the $BaMn_3Al_9O_{19}$ solid. For iron containing solids, up to 4 $Fe^{3+}$ cations may be introduced without destabilization of the structure. Finally, when both Fe and Mn cations are present, one iron cation limits the introduction of manganese to 2 cations only. However, all solids show exceptional thermal resistance because aging at 1200°C does not induce any structure change and does not lead to a drastic loss of SSA.

Catalytic activity in methane combustion is very low for the $BaAl_{12}O_{19}$ matrix. However, introduction of active ions, like $Fe^{3+}$ or $Mn^{3+}$, enhances strongly the activity. Optimum was found for $BaFe_2Al_{10}O_{19}$,

$BaMn_3Al_9O_{19}$ and $BaFeMnAl_{10}O_{19}$; the three solids have a light-off temperature close to 560–600°C. Both cations are active but it seems that iron is a little bit more active due to the presence of $Mn^{2+}$ ions in mixed oxides, as deduced from the determination of the intrinsic activities. For these three catalysts, aging has no effect except some surface area lowering and they may be selected as valuable candidates for high temperature catalytic combustion. In Japan, some hexaaluminates have been effectively used by Arai et al. [24] for catalytic gas turbines application, the honeycomb being constituted by pure Mn-substituted hexaaluminate.

## Acknowledgements

The authors are grateful to GAZ DE FRANCE, Direction de la Recherche, Département des Etudes Générales, Pôle Combustion Catalytique et Mécanique des Fluides, for the stimulating discussion and financial support as well as to the European Community for a grant from the Brite Euram project No. 5846.

## References

[1] D.L. Trimm, Appl. Catal. 7 (1983) 249.
[2] Z.R. Ismagilov, M.A. Kerzhentsev, Catal. Rev.-Sci. Eng. 32 (1990) 51.
[3] I. Stambler, Gas Turbine World 32 (1993) 32.
[4] M.F.M. Zwinkels, S.G. Jaras, P.G. Menon, T.A. Griffin, Catal. Rev.-Sci. Eng. 35 (1993) 319.
[5] K. Wefers, C. Misra, Oxides and hydroxides of aluminum, Alcoa Technical Paper No. 19 (revised), Alcoa Laboratories, 1987, pp. 40–42.
[6] A.F. Wells, Structural Inorganic Chemistry, 3rd Edition, Oxford University Press, Oxford, 1962, p. 480 (Chapter XII).
[7] D.F. Shriver, P.W. Atkins, C.H. Langford, Inorganic Chemistry, Oxford University Press, Oxford, 1990, p. 590.
[8] R. Stevens, J.G.P. Binner, J. Mater. Sci. 19 (1984) 695.
[9] M.K. Cinibulk, J. Mater. Sci. Lett. 14 (1995) 651.
[10] M. Machida, K. Eguchi, H. Arai, J. Catal. 103 (1987) 385.
[11] H. Arai, K. Eguchi, M. Machida, Proceedings of the MRS International Meeting on Advanced Materials, Vol. 2, 1989, pp. 243–253.
[12] M. Machida, K. Eguchi, H. Arai, Bull. Chem. Soc. Jpn. 61 (1988) 3659.
[13] J.M. Millet, Ph.D. Thesis, No. 259-90, Université Claude Bernard, Lyon, 1990.
[14] C.K Jorgensen, Absorption Spectra and Chemical Bonding in Complexes, Pergamon Press, Oxford, 1964, p. 285.
[15] S. Kimura, S. Bannai, I. Shindo, Mater. Res. Bull. 17 (1982) 209.
[16] B. Beguin, E. Garbowski, M. Primet, J. Catal. 127 (1991) 595.
[17] G. Groppi, M. Bellotto, C. Christiani, P. Forzatti, Inter. Ceram. J. 94 (1994) 20.
[18] T.R.N. Kutty, M. Nayak, Mater. Res. Bull. 30 (1995) 3325.
[19] R.D. Shannon, C.T. Prewitt, Acta Crystallogr. B 25 (1969) 925.
[20] R.D. Shannon, C.T. Prewitt, Acta Crystallogr. B 26 (1970) 1046.
[21] D. Naoufal, J.M. Millet, E. Garbowski, Y. Brullé, M. Primet, Catal. Lett. 54 (1998) 141.
[22] P. Artizzu, E. Garbowski, M. Primet, Y. Brullé, J. Saint-Just, Catal. Today 47 (1999) 83.
[23] G. Groppi, C. Cristiani, P. Forzatti, J. Catal. 168 (1998) 95.
[24] H. Arai, M.K. Eguchi, M. Machida, Proceedings of Fukuoka International Symposium, Vol. 20, 1990, pp. 227–236.